Title: The role of viral interference in shaping RSV epidemics following the 2009 H1N1 influenza pandemic

Authors: Ke Li[1]*, Deus Thindwa[1], Daniel M Weinberger[1], Virginia E Pitzer[1]*

Affiliations:

[1]Department of Epidemiology of Microbial Diseases, Yale School of Public Health, New Haven, CT, USA.

*Corresponding authors. ke.li.kl662@yale.edu, virginia.pitzer@yale.edu

One Sentence Summary: We demonstrated disrupted RSV activity in the United States following the 2009 influenza pandemic by analyzing weekly positive tests for RSV and the pandemic H1N1 virus. During the 2009/10 season, RSV experienced reduced activity, which was negatively associated with the activity of pandemic influenza. In contrast, RSV showed increased activity in the 2010/11 season due to the buildup of susceptible populations from the previous season. By focusing on the dynamics of RSV following the pandemic, we found evidence supporting interactions between the viruses at the population level. Our findings suggest that infections with pandemic influenza could: 1) reduce host susceptibility to RSV coinfection, 2) shorten the RSV infectious period in coinfected individuals, or 3) decrease RSV infectivity in coinfection.

Abstract: Respiratory syncytial virus (RSV) primarily affects infants, young children, and older adults, with seasonal outbreaks in the United States (US) peaking around December or January. Despite the limited implementation of non-pharmaceutical interventions, disrupted RSV activity was observed in different countries following the 2009 influenza pandemic, suggesting possible viral interference from influenza. Although interactions between the

influenza A/H1N1 pandemic virus and RSV have been demonstrated at an individual level, it remains unclear whether the disruption of RSV activity at the population level can be attributed to viral interference. In this work, we first evaluated changes in the timing and intensity of RSV activity across 10 regions of the US in the years following the 2009 influenza pandemic using dynamic time warping. We observed a reduction in RSV activity following the pandemic, which was associated with intensity of influenza activity in the region. We then developed an age-stratified, two-pathogen model to examine various hypotheses regarding viral interference mechanisms. Based on our model estimates, we identified three mechanisms through which influenza infections could interfere with RSV: 1) reducing susceptibility to RSV coinfection; 2) shortening the RSV infectious period in coinfected individuals; and 3) reducing RSV infectivity in coinfection. Our study offers statistical support for the occurrence of atypical RSV seasons following the 2009 influenza pandemic. Our work also offers new insights into the mechanisms of viral interference that contribute to disruptions in RSV epidemics and provides a model-fitting framework that enables the analysis of new surveillance data for studying viral interference at the population level.

Main Text:

INTRODUCTION

Respiratory syncytial virus (RSV) infections are a major public health concern for infants and young children, causing severe lower respiratory tract infections (*1*, *2*). In 2019, an estimated 13,300 deaths were associated with RSV-induced acute lower respiratory infections in hospitals, and there were 45,700 RSV-attributed deaths in infants aged 0-6 months worldwide (*3*). In the United States (US) and other temperate regions, RSV activity is strongly seasonal, typically beginning in the fall and peaking in winter (*4*). During the COVID-19 pandemic in 2020-2021, RSV disappeared for more than a year in the Northern Hemisphere then reemerged

out of the normal season (*5*, *6*). This was likely due to the implementation of non-pharmaceutical interventions (NPIs) to reduce the spread of SARS-CoV-2. However, disruptions to RSV activity were also observed following the 2009 influenza pandemic in different countries despite the limited implementation of NPIs (*7–12*). Viral interference from the novel 2009 A/H1N1 influenza pandemic (pdmH1N1) virus was suggested as a cause of the delayed RSV activity.

Viral interference refers to a phenomenon where one virus prevents or reduces infection by another virus (*13*). Several possible mechanisms of interference have been proposed at the within-host level (*14–16*). Direct competition between viruses for infection of susceptible cells can result in viral interference, such that the consumption of target cells by one virus limits infection by the other. Viral interference can also occur through the host immune response. For example, antibody-mediated interference has been suggested as a mechanism for mitigating infection between genetically close viruses, such as RSV and human metapneumovirus (*16*). Host interferon responses (IFNs) have also been proposed as a mechanism leading to viral interference. Chan et al. demonstrated that ferrets infected with pdmH1N1 influenza A virus (IAV) could be protected from subsequent RSV infection depending upon the interval between the two infections. They showed that the protection was transient and mediated by the IFNs (*15*). More recently, viral interference between IAV and the SARS-CoV-2 was also studied using human airway epithelial cultures. Cheemarla et al. showed that IAV infection could lead to a robust IFN response that suppressed subsequent SARS-CoV-2 infection (*17*). In contrast, infection with SARS-CoV-2, which elicited a relatively weak immune response, was unable to suppress IAV infection, suggesting an asymmetric IFN-dependent viral interference mechanism.

While it is evident that viral interference occurs at the host level, demonstrating the presence of viral interference at the population level and quantifying its impact on disease transmission is more challenging. For example, co-infections with two or more viruses in an individual can potentially change the typical viral dynamics (e.g., time to infectiousness, symptoms and severity) in the host, leading to changes in disease transmission patterns at the population level, as reviewed in (*18*). To date, most studies that analyzed population-level viral interference have primarily focused upon statistical associations between reported positive cases of different viruses, using regression and correlation analyses (*16*, *19*). The method, lacking explicit mechanistic formulation, was unable to distinguish true viral interaction from other confounding factors, such as climate variables. Other techniques, including seasonal auto-regressive integrated moving average models (*20*) and Granger causality (*21*, *22*), have also been used to analyze time series of positive tests of viruses, aiming to identify potential interactions between viruses. However, neither the biological mechanisms underpinning potential viral interactions, nor the strength of interactions could be determined or quantified using these models.

Mathematical models that explicitly depict the underlying mechanisms of viral transmission have advantages in being able to integrate heterogeneous mechanisms and test different hypotheses (*23–25*). Some mathematical models have been proposed to study the effect of viral interference between RSV and influenza viruses at the population level and to quantify the interactions by fitting the models to incidence data (*26–28*). However, these models did not capture the natural infection history of RSV, which are characterized by intermediate immunity lying between perfectly and imperfectly immunizing infections (*29*). In this work, we started by analyzing laboratory-confirmed cases of RSV and the pdmH1N1 virus in different regions in the US. We applied a dynamic time warping and hierarchical clustering method to identify

atypical RSV seasons following the 2009 influenza pandemic. We then built a mechanistic, age-stratified mathematical model that incorporates an RSV transmission model into an influenza transmission model, coupled with hypothesized viral interference mechanisms. Using Latin Hypercube Sampling to explore the parameter space, we simulated various scenarios for influenza dynamics and quantified the potential interactions between RSV and pdmH1N1 influenza virus at the population level.

RESULTS

RSV activity following the 2009 influenza pandemic

RSV epidemics exhibit consistent seasonal timing and duration within each region of the US, with variation in timing between regions (**Fig. 1A** and **Fig. S1**). Annual RSV epidemics start in the fall and peak in the winter. Some regions (e.g., Regions 8 and 10 in the Upper Midwest and Northwest) exhibit biennial patterns, with RSV tending to start and peak earlier with a larger epidemic in even-numbered seasons (e.g., 2010/11 and 2012/13) compared to the odd-numbered years (e.g., 2009/10 and 2011/12). The influenza pandemic (the shaded area, **Fig. 1A** and **Fig. S1**) began in April 2009, after the 2008/09 RSV season (dashed black lines). This was followed by a second wave in most regions that started at the end of 2009, before the peak of the 2009/10 RSV season. In our analysis, we focus on RSV activity during the 2009/10 season, when the pdmH1N1 virus was the sole influenza virus circulating in the population, and the 2010/11 season following the pandemic.

Based on the laboratory reports of RSV-positive specimens (**Fig. 1A**), we quantified RSV activity following the pandemic season and in other normal epidemic seasons. Regions 1 and 4 (Northeast and Southeast) exhibited consistent annual patterns of RSV activity, with a steady onset and peak timing in different seasons, including the 2009/10 pandemic year (**Fig. 1B**).

However, we observed delayed RSV activity in 2010/11 compared with other seasons in the two regions, as indicated by a shift of intense RSV activity to later epidemic weeks. Again, Regions 8 and 10 showed a biennial pattern of RSV epidemics with an earlier onset and peak timing in even-numbered years (**Fig. 1B**). In these regions, delayed RSV activity was also evident in 2010/11 compared to other even-numbered years, and no notable shifts in the timing of RSV activity were observed in the 2009/10 season.

Clustering RSV activity using dynamic time warping

Epidemic curves often exhibit variations in reporting intervals and temporal dynamics, making it difficult to identify dissimilarities in disease spread patterns. To better identify and characterize potential time shifts in RSV activity following the pandemic, we used dynamic time warping (DTW) to compare RSV activity in the 2009/10 and the 2010/11 seasons with other epidemic seasons. The fundamental concept of DTW is to find the optimal alignment between multiple time series, allowing the adjustment of the timing of one of the time series while minimizing the distance between corresponding data points (*30*). An optimal alignment shows the indices of the elements in the query time-series that correspond to those in the reference time series (e.g., RSV time-series in the 2009/10 and 2010/11 seasons). The computed optimal alignment paths for RSV activity during the 2009/10 and 2010/11 seasons with respect to other seasons are provided in **Fig. S2**. We found that the alignment paths cross below the diagonal line for the 2010/11 season, indicating delayed RSV activity as depicted in **Fig. 1B**.

The hierarchical clustering results of seasonal RSV activity are given in **Fig. 2**. In Region 1 (**Fig. 2A**) and Region 4 (**Fig. 2B**), the seasons following the pandemic (i.e., 2009/10 and

2010/11) were closer in the dendrogram, grouped into the same cluster, compared with other seasons before or after the pandemic (as shown in the dashed box). This indicated more similar trends of RSV activity in these years. We also observed that even within the same cluster, the 2009/10 season (highlighted in blue) was distant from the 2010/11 season (highlighted in red), suggesting a different pattern between the two seasons following the pandemic. Notably, the hierarchical clustering method successfully captured the biennial pattern in Region 8 (**Fig. 2C**), Region 10 (**Fig. 2D**), and other regions in the US (**Fig. S3**), grouping even seasons and odd seasons into different clusters. Specifically, the 2009/10 season was grouped with even-year seasons in Region 8, indicating unusual RSV activity. While the 2010/11 season in Region 10 shares a cluster with other even-year seasons, its extended branch length in the dendrogram indicated a distinction from the other even-year seasons.

Linking RSV activity and the 2009 influenza pandemic

We further quantified RSV activity following the pandemic seasons across 10 regions of the US. Both the intensity and the center of gravity for each RSV epidemic season in each region were calculated. The onset time of RSV activity for each season was also calculated. There was a strong positive correlation (i.e., $\rho = 0.92$) between the center of gravity and onset time of RSV activity, indicating these two methods of measuring epidemic timing agree (see **Fig. S4**). We explored the trends of RSV activity in the 2009/10 and 2010/11 years across the US regions, assessing changes in both intensity and center of gravity in comparison to the median values of all other seasons in the same region (**Fig. 3**). Most regions in the US experienced decreased RSV intensity in the 2009/10 season, with the timing of RSV activity consistent with that of other seasons. By contrast, most regions in the US showed increased RSV intensity, with delayed peak timing in the 2010/11 season. We then computed the intensity of the pdmH1N1 virus, starting from April 2009 to May 2010. We found a negative association

between the intensity of RSV and the intensity of the pdmH1N1 virus (**Fig. 4A**)—enhanced influenza intensity was associated with decreased RSV intensity in the 2009/10 season (i.e., $\rho = -0.38$). The negative correlations between RSV activity and pdmH1N1 activity suggested the presence of viral interference from influenza on RSV transmission. No correlations were found between the intensity of the pdmH1N1 virus and the intensity of RSV (**Fig. 4B**) or the timing of RSV peak in 2010/11 (**Fig. S5**).

Transmission model analyses

To explore and examine various hypotheses on the mechanistic relationship between RSV activity and viral interference from influenza that might explain the statistical associations observed, we proposed a mathematical model that explicitly incorporated the transmission dynamics of RSV into that of the pdmH1N1 virus via three hypothetical viral interaction mechanisms (see **Materials and Methods** for detailed model description). We hypothesized that in hosts infected with pdmH1N1 virus, the IFN response leads to: 1) a reduction of the host's susceptibility to subsequent RSV infections (**Fig. S6A**), which was captured by a parameter θ; 2) a reduction of the infectious period of RSV co-infection (**Fig. S6B**), captured by a parameter η; and/or 3) a reduction of the force of infection of RSV (**Fig. S6C**), captured by a parameter ξ. Detailed model equations are provided in the **Supplementary Materials**.

The three proposed mechanisms were studied separately as Models I-III. For each mechanism, we first used Latin Hypercube Sampling (LHS) to generate a wide range of parameter values that allowed us to simulate different transmission dynamics of pandemic influenza in the 2009/10 season and explore the effects of viral interference (including the possibility of no interference when $\theta = 1$, $\eta = 1$ or $\xi = 1$). We then determined the goodness-of-fit of the models

based on the negative log-likelihood of the models fitted to the number of RSV-positive tests, and filtered the models to the top 2% best-fitting models to identify the corresponding parameter ranges for the viral interference mechanisms.

The best 2000 (i.e., top 2%) fitting models successfully captured the difference in relative intensity of RSV activity during the 2009/10 and the 2010/11 seasons; however, the best-fit models failed to capture the shift in timing of RSV activity during 2010/11. Based on the calculated likelihood, the model without viral interference (green curves in **Fig. 5**) was not included in the top 2% of models. The reduction of the host's susceptibility to RSV infection (Model I, **Fig. 5A**), the RSV infectious period (Model II, **Fig. 5B**), or the force of infection of RSV (Model III, **Fig. 5C**) led to decreased RSV activity in the 2009/10 season, followed by increased RSV cases in the 2010/11 season. The relative intensity of RSV activity between the two seasons could not be reproduced in the absence of viral interference mechanisms. Similar results were observed for the top 3% (**Fig. S7**) and top 5% **(Fig. S8**) of the models, such that the models also captured the relative intensity of RSV activity in the 2009/10 and 2010/11 seasons following the pandemic. Further, our models demonstrated that increased RSV activity in the 2010/11 season could be explained by an increase in the proportion of the population susceptible to RSV infection, as shown in **Fig. S9**.

The identified parameter spaces for θ, η and ξ from the top 2% best-fitting models for Region 1 provide insight into the effect of viral interference from influenza influencing RSV infection and transmission (**Fig. 6**). The median estimate for the reduction of host susceptibility to RSV infection when infected with influenza virus (θ) was 0.44 (95% CI: 0.23-0.60, **Fig. 6A**). In epidemiological terms, the median estimate for θ indicates that the presence of the pdmH1N1

infection reduces the likelihood of hosts being subsequently infected with RSV by nearly 60%. The median estimate for η implies the presence of the pdmH1N1 co-infection halves the RSV infectious period, i.e. increases the rate of recovery by a factor 1.98 (95% CI: 1.62-2.53, **Fig. 6B**). Similarly, the median estimate for ξ was 0.46 (95% CI: 0.20-0.80, **Fig. 6C**), suggesting the pdmH1N1 infection reduces RSV infectivity by 53%. The parameter distributions from the top 3% and top 5% of the fitted models were similar (**figs. S10-11**). Given the best-fit parameter distributions for the viral interference parameter excluding 1, our results suggest that viral interference plays a role in mediating the dynamics of RSV infection following influenza infection for all of the proposed mechanisms.

Our models were also able to capture the trends of RSV activity in Region 10 (showing a biennial RSV pattern) and Region 4 (where seasonal RSV activity is the earliest in the US). From the identified parameter space of the viral interaction terms, similar results were found showing strong viral interference between RSV and pdmH1N1 virus in Region 10 (**Fig. 6D-F**). The median estimate of the reduction in host susceptibility to RSV infection (θ) was 0.61 (95% CI: 0.42-0.74, **Fig. 6D**), the relative rate of recovery from co-infection (η) was 1.5 (95% CI: 1.28-2.22, **Fig. 6E**), and the relative RSV infectivity (ξ) was 0.62 (95% CI: 0.42-0.75, **Fig. 6F**). By contrast, we found weak interference effects between the viruses in Region 4, such that all estimated parameters were closed to 1 (**Figs. 6G-I**).

With the identified viral interference parameters, we further predicted the co-infection rate of RSV and pdmH1N1 influenza virus in different age groups following the pandemic in the presence or absence of viral interference. The rate was computed as the fraction of infections in each age group that were co-infections. We found that the presence of viral interference

reduced the co-infection rate in all age groups (**Fig. S12**). In particular, our model showed that the effect was even more profound at the young age groups (i.e., < 1 year old), reducing the co-infection rate from 2% to 0.8%. Such patterns could be explained by the age-specific likelihood of a susceptible individual coming into contact with an infectious individual.

DISCUSSION

By focusing on the dynamics of RSV following the 2009 H1N1 influenza pandemic, we found evidence supporting the presence of interactions between the viruses at the population level and examined the underlying mechanisms. This was accomplished using statistical analysis of laboratory-confirmed positive tests of both viruses in 10 regions of the US and a mathematical modeling approach. Using a dynamic time warping and hierarchical clustering method, we identified atypical RSV activity following the 2009 influenza pandemic. The results support and contribute to the current knowledge from several observational studies that RSV activity was disrupted following the pandemic (*7*–*12*). We further showed there was a negative correlation between the intensity of RSV and pdmH1N1 activity during the pandemic. Using a two-pathogen, age-stratified transmission model, we assessed potential interactions between the viruses and identified three mechanisms of viral interference that can replicate the relative difference of RSV activity in the two epidemic seasons following the pandemic. The identified parameter space suggested that infection with the pdmH1N1 virus could reduce either the host's susceptibility to a subsequent RSV infection, or the infectious period of RSV infection, or RSV infectivity.

Although the presence of viral interference between different pathogens is evident at the host level (*15*, *31*, *32*), demonstrating the impact of this phenomenon at the population poses a

significant challenge. Mechanistic models provide a valuable approach for dissecting the casual relationship among different components, integrating heterogeneous mechanisms and testing various hypotheses. One of the most important applications of mechanistic models is to estimate key parameters, as reviewed in (*33*). Parameter identifiability for data fitting is an important but unresolved challenge in modeling work due to model complexity or limited time-series on numerous quantities of interest (*34–36*). Waterlow et al. have previously highlighted the importance of parameter identifiability (*26*). They conducted a simulation and back-estimation study to evaluate the plausible parameter space of viral interaction parameters in an RSV-influenza model. By fitting the model to a single season of simulated data, however, they demonstrated that the inference results for the interaction parameters were often imprecise, indicated by large credible intervals. By contrast, we specifically focused on the RSV-pdmH1N1 pair in our study. During the 2009/10 epidemic season, the pdmH1N1 virus emerged as the only circulating influenza virus, dominating the population. The outbreak of pdmH1N1 virus provided an opportunity to investigate viral interference between pdmH1N1 and RSV. With the availability of regional-level data, we were able to dissect variations in the temporal dynamics (i.e., annual/biennial patterns) of RSV activity in different regions in the US and estimate the interaction parameters between the viruses. A key finding of the models suggests that the strength of interaction between the viruses could be estimated from surveillance data of both viruses in such situations, revealing that the activity of pdmH1N1 has an appreciable impact on RSV activity.

At the individual level, the host interferon response has been shown to be the mechanism underpinning viral interference between RSV and the pdmH1N1 virus (*15*). Depending upon the interval between pdmH1N1 and RSV infections, the within-host viral production of RSV could be completely suppressed, reduced, delayed, or shortened. Based on the within-host RSV

297 viral dynamics, we proposed three mechanisms through which innate immunity, stimulated by
298 the pdmH1N1 virus, could modulate the following RSV coinfection. The model fits showed
299 that each of the three mechanisms could successfully recapitulate a decrease in RSV activity,
300 followed by an enhanced RSV epidemic, in the two seasons following the pandemic. Our model
301 demonstrated that the increased intensity of the 2010/11 RSV season could be attributed to an
302 increased proportion of susceptible individuals in the population. Baker et al. similarly showed
303 that population susceptibility to influenza and RSV infections increased during the COVID-19
304 pandemic, leading to larger outbreaks following the relaxation of NPIs (*37*). More recently,
305 Lowensteyn et al. showed that the unprecedented RSV epidemic following the COVID-19
306 pandemic in the Netherlands was associated with waning immunity to RSV due to low
307 circulation of RSV during the NPIs period (*38*).

308

309 We note that none of the mechanisms considered in the model, including the null model (i.e.,
310 no viral interference), could capture the shift in timing of the 2010/11 RSV epidemic. One
311 possible explanation would be that we only assumed a transient viral interference interval
312 lasting up to a week, occurring in co-infected individuals and disappearing when the infection
313 resolves. The IFN response was not explicitly considered in our model, and could persist
314 slightly longer than the influenza infectious period. Although previous studies have suggested
315 that cross-protection following influenza infection against RSV could last more than two weeks
316 (*39*), this was not demonstrated in a ferret model, which shares several similarities with the
317 respiratory tracts of humans (*40*). The duration of cross-protection between RSV and the
318 pdmH1N1 virus only lasted a week in ferrets, as shown in (*15*).

319

Delayed RSV activity in the 2010/11 season could also be explained by the circulation of other respiratory viruses (e.g., rhinovirus and influenza B virus), which our model did not explicitly include. Here, our focus was not on exploring virus interactions among multiple influenza strains and RSV in general. Instead, our specific emphasis was on studying viral interference from the pdmH1N1 virus on RSV infection, where the interactions are evident at the host level. This focus was guided by experimental studies indicating that the genetic strains of influenza viruses elicit varying levels of host immunity (*41*). We also assumed that the RSV-influenza interaction was unidirectional during the 2009/10 season, meaning that only the pdmH1N1 virus would exhibit interference on RSV. This assumption is justified considering that the influenza pandemic preceded the normal 2009/10 RSV season, and our analysis focused on the disruption in RSV activity following the 2009 influenza pandemic. Note that neither could, nor did we intend to show the absence of viral interference from RSV against influenza viruses. To study viral interference from RSV in shaping the transmission dynamics of influenza may require time-series data from multiple epidemic seasons, as shown in a modeling study (*27*).

Besides potential viral interference, other factors can also change disease transmission patterns, leading to the variations between model predictions and the surveillance data. Behavioral changes can have significant impacts on viral circulation and transmission patterns, as observed during the COVID-19 pandemic (*42*). After the implementation of NPIs, there was a sharp decline in the number of positive RSV tests, and RSV activity remained disrupted in the following seasons (*5*, *43*). It is not clear how much of a role, if any, viral interference from SARS-CoV-2 played in disrupting RSV activity. Understanding the interplay of the effects of NPIs and viral interference is important to evaluate the role of behavioral and immunological factors more accurately on disease transmission. Additionally, environmental factors such as temperature and humidity (*29*) and vaccination coverage (*44*) can also play roles in shaping the

345 trajectory of disease spread. Incorporation of these factors into the dynamic model can be
346 improved in future work upon data availability.

347

348 Dynamic time warping (DTW) is a widely used statistical algorithm (*30*, *45*), but its application
349 in identifying various disease transmission patterns has been limited. Recently, multiple studies
350 have used DTW to analyze the trajectories of COVID-19 in different countries, aiming to
351 identify, cluster and predict future trends in disease transmission (*46–49*). Here, we utilized
352 DTW to examine and visualize similarities of RSV time-series, yielding clusters of RSV
353 activity before and after the 2009 influenza pandemic in the ten different regions of the US.
354 The method successfully identified the biennial pattern of RSV epidemics in certain regions of
355 the US and atypical RSV seasons following the pandemic. The graphical representation of
356 clusters based on DTW provides an accessible and interpretable method for comparing both
357 temporal and spatial time-series of incidence data, enhancing our understanding of disease
358 transmission patterns longitudinally or geographically. The DTW method also has a promising
359 potential for detecting and identifying atypical epidemic seasons.

360

361 We identified three plausible viral interference mechanisms that could shape RSV epidemics
362 following the influenza pandemic. We do acknowledge that these mechanisms are not mutually
363 exclusive. This raises the question of what kind of data would be needed to further distinguish
364 among the models and examine the relative importance of each mechanism for RSV
365 transmission. One possible direction would be to emphasize the incidence of coinfections over
366 a period of time. By fitting the prevalence of coinfections to mathematical models, we could
367 estimate essential kinetic parameters separately, such as the force of infection or the recovery
368 rate from the coinfected components. The comparison between these estimated parameter

values and the baseline values (i.e., the rates from individuals infected with one virus) helps discern different mechanisms and evaluate the relative contribution of each process.

Our study provides statistical and mathematical support for the presence of viral interference between the pdmH1N1 influenza virus and RSV at the population level. Multiple mechanisms mediated by the host immune response are capable of explaining RSV transmission dynamics following the 2009 influenza pandemic. Given the experimental support for within-host interference between RSV and influenza through IFN responses, all of these mechanisms could contribute to shaping RSV epidemics. The results have implications for implementing and evaluating disease control interventions. For example, mitigation measures that effectively decrease disease transmission could decrease the epidemic size in the current season but potentially lead to a larger outbreak in the following season, even if the measures are applied for only a week (i.e., transient protection). Hence, it is imperative to deliberate upon the optimal degree of disease suppression and the duration for which interventions should be applied prior to their implementation, as discussed in (*50*).

There are some limitations to our study. First, we did not have age information on the positive tests for RSV and influenza over time. Therefore, we assumed a well-mixed population and did not account for varying levels of immunity across different age groups beyond the age-specific contract matrices. It is possible that influenza virus stimulates a weaker innate immune response in young children compared to other age groups (*51*). In our model, the estimated interference parameters are interpreted as the average effects of viral interaction across the entire population. Although our model cannot be used to assess the strength of viral interference in each age group, our results are still sufficient to demonstrate the presence of viral

interference between pdmH1N1 and RSV within the population in general. Another limitation of our analyses is that our model did not take into account other circulating pathogens (e.g., rhinovirus or human parainfluenza virus) due to the added complexity and additional parameters required. For example, interference between rhinovirus and influenza viruses was recognized by epidemiological observations (*31*), and the delayed 2009 influenza pandemic in Europe was attributed to the prevalence of rhinovirus (*7*). The analysis of viral interference between the pandemic influenza virus and other viruses will be left for future work. Additionally, our model estimates did not show strong viral interference effects between the viruses in Region 4. The difference in the estimates of viral interference for Region 4 is likely attributable to the different pdmH1N1 activity in this region. In Regions 1 and 10, there was a strong second wave of pdmH1N1 before the 2009/10 RSV season, whereas the second pdmH1N1 wave was not observed in Region 4. It is not clear why the pandemic influenza exhibited different activity in these regions.

Our findings, which indicate an association between the incidence of RSV infections and pdmH1N1 infections, also have implications for enhanced surveillance of disease transmission of other viruses. As other respiratory viruses (e.g., seasonal influenza viruses and SARS-CoV-2) are expected to co-circulate in the upcoming epidemic seasons, our study provides a framework for studying viral interactions and understanding transmission dynamics. Additional information on the frequency of RSV and other viruses, along with coinfections, would enable us to further validate our results. The mechanistic model proposed in this work is flexible to incorporate the effects of vaccination in preventing disease, such as introducing a model compartment that is resistant to infection and becomes susceptible over time. The extended model can be used for the evaluation of various vaccination scenarios, assessing the impact of vaccination coverage on long-term disease patterns while considering the presence

of viral interference. Through systematic analysis of these scenarios, our model can provide valuable insights into the dynamic interplay between vaccination strategies and the patterns of disease transmission, contributing to informed decision-making in public health interventions.

MATERIALS AND METHODS

Laboratory reporting of RSV and influenza

Weekly data on laboratory reporting of RSV tests in ten Health and Human Services (HHS) regions in the US from June 2007 to July 2019 were obtained from The National Respiratory and Enteric Virus Surveillance System (https://data.cdc.gov/Laboratory-Surveillance/Respiratory-Syncytial-Virus-Laboratory-Data-NREVSS/52kb-ccu2/about_data). The regional map can be found on the https://www.hhs.gov/about/agencies/iea/regional-offices/index.html website. Positive RSV tests were detected using three diagnostic methods: 1) antigen detection; 2) reverse transcription polymerase chain reaction (RT-PCR); and 3) viral culture. Correspondingly, the data on laboratory reporting of influenza tests in the US from the same period were obtained from the Center for Disease Control and Prevention (CDC) website https://gis.cdc.gov/grasp/fluview/flu_by_age_virus.html.

The raw laboratory data were rescaled based on the number of positive tests to account for variations in testing practices over time (*29*). We first calculated a one-year moving average of the weekly number of RSV or influenza tests (both positive and negative tests) in each region centered on each week. We then calculated a weekly scaling factor for each region equal to the average number of RSV or influenza tests during the entire period of reporting (i.e., 12 epidemic seasons from 2007-2019) divided by the one-year moving average. The rescaled number of RSV or influenza-positive tests for each region was then calculated as the reported

number of positive tests multiplied by the weekly scaling factor. The rescaled data for RSV and influenza are shown in **Fig. 1** and **S1.**

Demographic Data

Information about population size in each age group was obtained from the US Census Bureau's American Community Survey. Birth rates varied between regions and over time based on the crude annual birth rate for each HSS region from 1990 to 2019. These were obtained from https://wonder.cdc.gov/controller/datarequest/D66. To capture aging among infants and children more accurately in our mathematical model, we divided the <1 year and 1-4 years age class into 12-month age groups. The remaining population was divided into 5 classes: 5-9 years, 10-19 years, 20-39 years, 39-60 years and >60 years old. Individuals were assumed to age exponentially into the next age class, with the rate of aging equal to the multiplicative inverse of the width of the age class.

The onset timing, center of gravity, and intensity of RSV activity

To determine the onset timing (measured by week) of each seasonal RSV epidemic for each region, we initially fitted a p-spline curve to the RSV incidence data. We then calculated the first and second derivatives of the fitted curve. The onset timing corresponds to the time point at which the second derivative of the fitted p-spline curve reaches its maximum value during the increasing segment of the first derivative (*52*). The center of gravity of RSV activity for each season in each region ($G_{s,r}$) was measured as the mean epidemic week, with each week weighted by the number of positive tests, such that $G_{s,r} = \sum_{w\in[1:52]} w \times Y_{s,r,w} / \sum_{w\in[1:52]} Y_{s,r,w}$, where w is an index for the week of each epidemic year, and $Y_{s,r,w}$ is the number of rescaled positive RSV tests in region r during epidemic season s and week w. To

466 determine the RSV intensity for each season and region, we also used the fitted p-spline curve.
467 The epidemic peak timing was determined at the point when RSV activity reaches its
468 maximum. The intensity of RSV was calculated as the fraction of positive tests before the
469 epidemic peak timing, corresponding to the integral of the positive first derivative of the log-
470 transformed fitted p-spline curve.

471

472 **Dynamic time warping and hierarchical clustering**

473

474 We used a dynamic time warping (DTW) (see a review for details (*53*)) to calculate the
475 pairwise non-linear alignment of the 12 RSV time-series (corresponding to the 12 seasons) in
476 each region of the US (**Fig. S2**) and quantify dissimilarity between those time-series. The DTW
477 algorithm computed the optimum warping path between two series under certain constraints,
478 including monotonicity, continuity, warping window, and boundary (*53*). The R packages *dtw*
479 and *dtwclust* facilitated the implementation of the algorithm and optimization (*54*).

480

481 After calculating distances, a local cost matrix (*lcm*) was generated with dimensions of $n \times m$,
482 where n and m represent the lengths of the pairwise time series. Considering the input time
483 series Q and S, for each element (i, j) of the *lcm*, the distance between Q_i and R_j was computed,
484 such that $lcm(i,j) = (\sum |Q_i - R_j|^p)^{1/p}$. The DTW algorithm thereby identifies the path that
485 minimizes the alignment between pairwise time-series Q and R by iteratively stepping through
486 the *lcm*, starting at $lcm(1,1)$ and finishing at $lcm(n,m)$, while aggregating the cost. At each
487 step, the algorithm determines the direction in which the cost increases the least under the given
488 constraints.

489

To limit the area of the *lcm* that the DTW algorithm must traverse, we implemented the Sakoe-Chiba window as a global constraint (*54*). This constraint confines the allowed region along the diagonal of the *lcm*. To select an optimal window size for hierarchical clustering, we evaluated clustering using the modified Davies-Bouldin (DB) internal cluster validity index (CVI), iterating across different values of window size from 1 to 52, corresponding to 1 to 52 weeks, while keeping cluster size as 3. For each window size, the DB CVI calculated distances from computed cluster centroids

We subsequently performed hierarchical clustering on the distances of aligned time-series using DTW. We utilized the Ward D2 clustering method, which minimizes the sum of squared differences from the centroid during the merging of clusters. This hierarchical clustering of the 12 RSV epidemics in each region created a hierarchy of groups. As the level in the hierarchy increased, clusters were formed by merging clusters from the next lower level, resulting in an ordered sequence of groupings.

Transmission dynamic models

We used an age-stratified Susceptible-Infected-Susceptible (SIS) model, taking into account repeat infections, to describe the transmission dynamics of RSV. The model was initially proposed by Pitzer et al. (*29*) to study the environmental drivers of the spatiotemporal dynamics of RSV in the US. The model assumed individuals were born with protective maternal immunity, which waned exponentially, leaving the infants susceptible to infection. We assumed a progressive build-up of immunity following up to four previous infections. Following infection with RSV, individuals developed partial immunity, reducing the rate of subsequent infection and relative infectiousness of the following infections. We also assumed

subsequent infections had a shortened recovery time compared to primary infections. Transmission-relevant contact patterns were assumed to be frequency-dependent and were consistent with the previous work (*29*). The model was able to reproduce the seasonal annual or biennial patterns of RSV transmission in different regions of the US. To model influenza transmission dynamics, we used a Susceptible-Infected-Recovered-Susceptible (SIRS) model. We assumed waning immunity for recovered individuals, allowing influenza infection to recur following the influenza pandemic in the 2009/10 and 2010/11 seasons.

The RSV and influenza transmission models were coupled through three hypothetical viral interference mechanisms. The first mechanism assumed influenza infection reduced the host's susceptibility to subsequent RSV coinfections, modulating the infection rate of susceptible individuals (**Fig. S6A**), captured by a parameter θ, i.e. $dX_{si}/dt = -\theta\lambda_1 X_{si} + \lambda_2 X_{ss} - \gamma_2 X_{si}$ (Eq. (10) in **Supplementary Materials**). The second mechanism assumed influenza infection reduced the infectious period (i.e. increased the rate of recovery) of subsequent RSV coinfections (**Fig. S6B**), captured by a parameter η, i.e. $dX_{i1i}/dt = -\eta\gamma_1 X_{ii} + \lambda_1 X_{si} + \lambda_2 X_{is} - \gamma_2 X_{ii}$ (Eq. (11) in **Supplementary Materials**). The third mechanism assumed influenza infection reduced the force of infection of RSV (**Fig. S6C**), captured by a parameter ξ, i.e. $\lambda_1 = \xi\beta_1(t)X_{ai}$, where $X_{ai,\ a=\{i1,i2,i3,i4\}}$ represents coinfection terms. The model was described by a system of ordinary differential equations (ODEs); see **Supplementary Materials** for details.

Model calibration

To calibrate the model parameters, we first fit the RSV dynamic model to the laboratory reports of positive RSV specimens from 2007 to 2019. We estimated the seasonal amplitude (α_1),

539 seasonal offset (ϕ_1) and reporting fraction (f) for each region, respectively, using maximum
540 likelihood estimation. The likelihood of the data given the model was calculated by assuming
541 the number of positive cases in each week was Poisson-distributed with a mean equal to the
542 model-predicted cases times the reporting fraction. Other parameter values for the model were
543 adopted from (*29*), and are provided in Table 1 in the **Supplementary Materials**. For the
544 influenza model, we assumed the mean infectious period for primary and secondary influenza
545 infections is 8 days (*55*), the duration of waning immunity is 40 weeks, and the seasonal
546 amplitude is equal to that estimated for RSV. We started by simulating only the RSV epidemic
547 model, seeding the model with one RSV-infected individual in each age group except the <1
548 year-old age group. We used a burn-in period of 60 or 61 years, depending upon the region that
549 exhibits either an annual or biennial RSV pattern, to ensure the RSV model reached an
550 equilibrium quasi-steady state. Influenza infection was introduced to the population after the
551 model reached the equilibrium quasi-steady state.

552

553 To probe the effects of viral interference from pdmH1N1 infection on shaping RSV epidemics,
554 we applied Latin Hypercube Sampling (LHS) to generate representative samples from a wide
555 range of values for the parameter space $\Phi = (\Theta, \beta_2, \phi_2, \tau)$, where $\Theta = (\theta, \xi, \eta)$ represents
556 interference parameters; β_2 is the transmission rate of the pdmH1N1 virus; ϕ_2 is the seasonal
557 phase offset of influenza dynamics, and τ is the time point when influenza infection is seeded
558 in the population. We generated 100,000 samples from a uniform distribution $U(0,1)$ for the
559 parameter θ and ξ, respectively, and from a uniform distribution $U(1,3)$ for the parameter η.
560 We also sampled 100,000 values from a uniform distribution $U(100,110)$ for the parameter τ,
561 mimicking the onset time of the second H1N1 pandemic wave during the winter of 2009.
562 Additionally, 100,000 samples were obtained from a uniform distribution $U(2,3)$ for the

parameter β_2, based on the estimates of the basic reproduction number of the H1N1 pandemic virus in the United States (*56*). 100,000 values of seasonal offset of influenza ϕ_2 were sampled from a uniform distribution $U(-1,1)$.

Next, we explored the parameter space for each viral interference mechanism separately. We generated forward simulations using the sampled 100,000 parameter sets and calculated the likelihood to evaluate the "goodness-of-fit" of the model. The data that we used was the weekly RSV positive tests in the 2009/10 season in Region 1 (CT: Connecticut, ME: Maine, MA: Massachusetts, NH: New Hampshire, RI: Rhode Island, and VT: Vermont), Region 4 (AL: Alabama, FL: Florida, GA: Georgia, KY: Kentucky, MS: Mississippi, NC: North Carolina, SC: South Carolina, and TN: Tennessee) or Region 10 (AK: Alaska, ID: Idaho, OR: Oregon, and WA: Washington), respectively. We focused on the 2009/10 season data because that was the season when only the pdmH1N1 virus circulated in the population. We used the following 2010/11 season for model validation. For each set of parameters, the likelihood of the data given the model was calculated by assuming the number of positive cases in each week was Poisson-distributed with a mean equal to the model-predicted cases divided by corresponding weekly scaling factors. We ranked the negative likelihood in an ascending order and determined the distributions of parameter values (θ, ξ, η) based on the top 2% (i.e., the first 2000) models.

List of Supplementary Materials

Supplementary Figures: Fig. S1 to S12 (pdf file)

Supplementary Materials (pdf file)

587 **Reference**

588 1. M. Tin Tin Htar, M. S. Yerramalla, J. C. Moïsi, D. L. Swerdlow, The burden of respiratory
589 syncytial virus in adults: a systematic review and meta-analysis. *Epidemiol. Infect.* **148**,
590 e48 (2020).

591 2. T. Shi, D. A. McAllister, K. L. O'Brien, E. A. F. Simoes, S. A. Madhi, B. D. Gessner, F. P.
592 Polack, E. Balsells, S. Acacio, C. Aguayo, I. Alassani, A. Ali, M. Antonio, S. Awasthi, J.
593 O. Awori, E. Azziz-Baumgartner, H. C. Baggett, V. L. Baillie, A. Balmaseda, A.
594 Barahona, S. Basnet, Q. Bassat, W. Basualdo, G. Bigogo, L. Bont, R. F. Breiman, W. A.
595 Brooks, S. Broor, N. Bruce, D. Bruden, P. Buchy, S. Campbell, P. Carosone-Link, M.
596 Chadha, J. Chipeta, M. Chou, W. Clara, C. Cohen, E. de Cuellar, D.-A. Dang, B. Dash-
597 Yandag, M. Deloria-Knoll, M. Dherani, T. Eap, B. E. Ebruke, M. Echavarria, C. C. de
598 Freitas Lázaro Emediato, R. A. Fasce, D. R. Feikin, L. Feng, A. Gentile, A. Gordon, D.
599 Goswami, S. Goyet, M. Groome, N. Halasa, S. Hirve, N. Homaira, S. R. C. Howie, J.
600 Jara, I. Jroundi, C. B. Kartasasmita, N. Khuri-Bulos, K. L. Kotloff, A. Krishnan, R.
601 Libster, O. Lopez, M. G. Lucero, F. Lucion, S. P. Lupisan, D. N. Marcone, J. P.
602 McCracken, M. Mejia, J. C. Moisi, J. M. Montgomery, D. P. Moore, C. Moraleda, J.
603 Moyes, P. Munywoki, K. Mutyara, M. P. Nicol, D. J. Nokes, P. Nymadawa, M. T. da
604 Costa Oliveira, H. Oshitani, N. Pandey, G. Paranhos-Baccalà, L. N. Phillips, V. S. Picot,
605 M. Rahman, M. Rakoto-Andrianarivelo, Z. A. Rasmussen, B. A. Rath, A. Robinson, C.
606 Romero, G. Russomando, V. Salimi, P. Sawatwong, N. Scheltema, B. Schweiger, J. A.
607 G. Scott, P. Seidenberg, K. Shen, R. Singleton, V. Sotomayor, T. A. Strand, A. Sutanto,
608 M. Sylla, M. D. Tapia, S. Thamthitiwat, E. D. Thomas, R. Tokarz, C. Turner, M. Venter,
609 S. Waicharoen, J. Wang, W. Watthanaworawit, L.-M. Yoshida, H. Yu, H. J. Zar, H.
610 Campbell, H. Nair, RSV Global Epidemiology Network, Global, regional, and national
611 disease burden estimates of acute lower respiratory infections due to respiratory
612 syncytial virus in young children in 2015: a systematic review and modelling study.
613 *Lancet*. **390**, 946–958 (2017).

614 3. Y. Li, X. Wang, D. M. Blau, M. T. Caballero, D. R. Feikin, C. J. Gill, S. A. Madhi, S. B.
615 Omer, E. A. F. Simões, H. Campbell, A. B. Pariente, D. Bardach, Q. Bassat, J.-S.
616 Casalegno, G. Chakhunashvili, N. Crawford, D. Danilenko, L. A. H. Do, M. Echavarria,
617 A. Gentile, A. Gordon, T. Heikkinen, Q. S. Huang, S. Jullien, A. Krishnan, E. L. Lopez, J.
618 Markić, A. Mira-Iglesias, H. C. Moore, J. Moyes, L. Mwananyanda, D. J. Nokes, F.
619 Noordeen, E. Obodai, N. Palani, C. Romero, V. Salimi, A. Satav, E. Seo, Z. Shchomak,
620 R. Singleton, K. Stolyarov, S. K. Stoszek, A. von Gottberg, D. Wurzel, L.-M. Yoshida, C.
621 F. Yung, H. J. Zar, Respiratory Virus Global Epidemiology Network, H. Nair, RESCEU
622 investigators, Global, regional, and national disease burden estimates of acute lower
623 respiratory infections due to respiratory syncytial virus in children younger than 5 years
624 in 2019: a systematic analysis. *Lancet*. **399**, 2047–2064 (2022).

625 4. M. L. Boron, L. Edelman, J. R. Groothuis, F. J. Malinoski, A novel active respiratory
626 syncytial virus surveillance system in the United States: variability in the local and
627 regional incidence of infection. *Pediatr. Infect. Dis. J.* **27**, 1095–1098 (2008).

628 5. I. Kuitunen, M. Renko, Lessons to learn from the current pandemic for future non-
629 pharmaceutical interventions against the respiratory syncytial virus – nationwide
630 register-study in Finland. *Infect. Dis.* **53**, 476–478 (2021).

631 6. Z. Zheng, V. E. Pitzer, E. D. Shapiro, L. J. Bont, D. M. Weinberger, Estimation of the
632 Timing and Intensity of Reemergence of Respiratory Syncytial Virus Following the
633 COVID-19 Pandemic in the US. *JAMA Netw Open*. **4**, e2141779 (2021).

634 7. J. S. Casalegno, M. Ottmann, M. Bouscambert-Duchamp, M. Valette, F. Morfin, B. Lina,

635 Impact of the 2009 influenza A(H1N1) pandemic wave on the pattern of hibernal
636 respiratory virus epidemics, France, 2009. *Euro Surveill.* **15** (2010) (available at
637 https://www.ncbi.nlm.nih.gov/pubmed/20158981).

638 8. T. Meningher, M. Hindiyeh, L. Regev, H. Sherbany, E. Mendelson, M. Mandelboim,
639 Relationships between A(H1N1)pdm09 influenza infection and infections with other
640 respiratory viruses. *Influenza Other Respi. Viruses*. **8**, 422–430 (2014).

641 9. S. Hirsh, M. Hindiyeh, L. Kolet, L. Regev, H. Sherbany, K. Yaary, E. Mendelson, M.
642 Mandelboim, Epidemiological changes of respiratory syncytial virus (RSV) infections in
643 Israel. *PLoS One*. **9**, e90515 (2014).

644 10. N. Schnepf, M. Resche-Rigon, A. Chaillon, A. Scemla, G. Gras, O. Semoun, P.
645 Taboulet, J.-M. Molina, F. Simon, A. Goudeau, J. LeGoff, High burden of non-influenza
646 viruses in influenza-like illness in the early weeks of H1N1v epidemic in France. *PLoS*
647 *One*. **6**, e23514 (2011).

648 11. G. C. Mak, A. H. Wong, W. Y. Y. Ho, W. Lim, The impact of pandemic influenza A
649 (H1N1) 2009 on the circulation of respiratory viruses 2009-2011. *Influenza Other Respi.*
650 *Viruses*. **6**, e6–10 (2012).

651 12. L. Yang, K. H. Chan, L. K. P. Suen, K. P. Chan, X. Wang, P. Cao, D. He, J. S. M. Peiris,
652 C. M. Wong, Impact of the 2009 H1N1 Pandemic on Age-Specific Epidemic Curves of
653 Other Respiratory Viruses: A Comparison of Pre-Pandemic, Pandemic and Post-
654 Pandemic Periods in a Subtropical City. *PLoS One*. **10**, e0125447 (2015).

655 13. J. Piret, G. Boivin, Viral Interference between Respiratory Viruses. *Emerg. Infect. Dis.*
656 **28**, 273–281 (2022).

657 14. A. J. Gonzalez, E. C. Ijezie, O. B. Balemba, T. A. Miura, Attenuation of Influenza A Virus
658 Disease Severity by Viral Coinfection in a Mouse Model. *J. Virol.* **92** (2018),
659 doi:10.1128/JVI.00881-18.

660 15. K. F. Chan, L. A. Carolan, D. Korenkov, J. Druce, J. McCaw, P. C. Reading, I. G. Barr,
661 K. L. Laurie, Investigating Viral Interference Between Influenza A Virus and Human
662 Respiratory Syncytial Virus in a Ferret Model of Infection. *J. Infect. Dis.* **218**, 406–417
663 (2018).

664 16. S. Bhattacharyya, P. H. Gesteland, K. Korgenski, O. N. Bjørnstad, F. R. Adler, Cross-
665 immunity between strains explains the dynamical pattern of paramyxoviruses. *Proc.*
666 *Natl. Acad. Sci. U. S. A.* **112**, 13396–13400 (2015).

667 17. N. R. Cheemarla, T. A. Watkins, V. T. Mihaylova, E. F. Foxman, Viral Interference
668 During Influenza A–SARS-CoV-2 Coinfection of the Human Airway Epithelium and
669 Reversal by Oseltamivir. *J. Infect. Dis.*, jiad402 (2023).

670 18. L. Opatowski, M. Baguelin, R. M. Eggo, Influenza interaction with cocirculating
671 pathogens and its impact on surveillance, pathogenesis, and epidemic profile: A key
672 role for mathematical modelling. *PLoS Pathog.* **14**, e1006770 (2018).

673 19. S. Nickbakhsh, C. Mair, L. Matthews, R. Reeve, P. C. D. Johnson, F. Thorburn, B. von
674 Wissmann, A. Reynolds, J. McMenamin, R. N. Gunson, P. R. Murcia, Virus–virus
675 interactions impact the population dynamics of influenza and the common cold.
676 *Proceedings of the National Academy of Sciences*. **116**, 27142–27150 (2019).

677 20. W. Hendriks, H. Boshuizen, A. Dekkers, M. Knol, G. A. Donker, A. van der Ende, H.

Korthals Altes, Temporal cross-correlation between influenza-like illnesses and invasive pneumococcal disease in The Netherlands. *Influenza Other Respi. Viruses*. **11**, 130–137 (2017).

21. R. E. G. Upshur, R. Moineddin, E. J. Crighton, M. Mamdani, Interactions of viral pathogens on hospital admissions for pneumonia, croup and chronic obstructive pulmonary diseases: results of a multivariate time-series analysis. *Epidemiol. Infect.* **134**, 1174–1178 (2006).

22. K. P. Tao, M. K. C. Chong, K. Y. Y. Chan, J. C. S. Pun, J. G. S. Tsun, S. M. W. Chow, C. S. H. Ng, M. H. T. Wang, P. K. S. Chan, A. M. Li, R. W. Y. Chan, Suppression of influenza virus infection by rhinovirus interference - at the population, individual and cellular levels. *Curr. Res. Microb. Sci.* **3**, 100147 (2022).

23. N. C. Grassly, C. Fraser, Mathematical models of infectious disease transmission. *Nat. Rev. Microbiol.* **6**, 477–487 (2008).

24. F. Brauer, C. Castillo-Chavez, Z. Feng, *Mathematical Models in Epidemiology* (Springer New York).

25. L. Pinky, H. M. Dobrovolny, Epidemiological Consequences of Viral Interference: A Mathematical Modeling Study of Two Interacting Viruses. *Front. Microbiol.* **13**, 830423 (2022).

26. N. R. Waterlow, S. Flasche, A. Minter, R. M. Eggo, Competition between RSV and influenza: Limits of modelling inference from surveillance data. *Epidemics*. **35**, 100460 (2021).

27. N. R. Waterlow, M. Toizumi, E. van Leeuwen, H.-A. Thi Nguyen, L. Myint-Yoshida, R. M. Eggo, S. Flasche, Evidence for influenza and RSV interaction from 10 years of enhanced surveillance in Nha Trang, Vietnam, a modelling study. *PLoS Comput. Biol.* **18**, e1010234 (2022).

28. S. C. Kramer, J.-S. Casalegno, M. Domenech de Cellès, Characterizing the epidemiological interactions between influenza and respiratory syncytial viruses and their implications for epidemic control. *bioRxiv* (2022), , doi:10.1101/2022.11.29.22282872.

29. V. E. Pitzer, C. Viboud, W. J. Alonso, T. Wilcox, C. J. Metcalf, C. A. Steiner, A. K. Haynes, B. T. Grenfell, Environmental drivers of the spatiotemporal dynamics of respiratory syncytial virus in the United States. *PLoS Pathog.* **11**, e1004591 (2015).

30. H. Sakoe, S. Chiba, Dynamic programming algorithm optimization for spoken word recognition. *IEEE Trans. Acoust.* **26**, 43–49 (1978).

31. A. Wu, V. T. Mihaylova, M. L. Landry, E. F. Foxman, Interference between rhinovirus and influenza A virus: a clinical data analysis and experimental infection study. *Lancet Microbe*. **1**, e254–e262 (2020).

32. M. C. Swets, C. D. Russell, E. M. Harrison, A. B. Docherty, N. Lone, M. Girvan, H. E. Hardwick, L. G. Visser, P. J. M. Openshaw, G. H. Groeneveld, M. G. Semple, J. K. Baillie, SARS-CoV-2 co-infection with influenza viruses, respiratory syncytial virus, or adenoviruses. *Lancet*. **399**, 1463–1464 (2022).

33. A. Handel, L. E. Liao, C. A. A. Beauchemin, Progress and trends in mathematical modelling of influenza A virus infections. *Current Opinion in Systems Biology*. **12**, 30–36

(2018).

34. N. Tuncer, H. Gulbudak, V. L. Cannataro, M. Martcheva, Structural and Practical Identifiability Issues of Immuno-Epidemiological Vector-Host Models with Application to Rift Valley Fever. *Bull. Math. Biol.* **78**, 1796–1827 (2016).

35. N. Tuncer, M. Marctheva, B. LaBarre, S. Payoute, Structural and Practical Identifiability Analysis of Zika Epidemiological Models. *Bull. Math. Biol.* **80**, 2209–2241 (2018).

36. Y.-H. Kao, M. C. Eisenberg, Practical unidentifiability of a simple vector-borne disease model: Implications for parameter estimation and intervention assessment. *Epidemics*. **25**, 89–100 (2018).

37. R. E. Baker, S. W. Park, W. Yang, G. A. Vecchi, C. J. E. Metcalf, B. T. Grenfell, The impact of COVID-19 nonpharmaceutical interventions on the future dynamics of endemic infections. *Proceedings of the National Academy of Sciences*. **117**, 30547–30553 (2020).

38. Y. N. Löwensteyn, Z. Zheng, N. Rave, M. A. G. E. Bannier, M.-N. Billard, J.-S. Casalegno, V. E. Pitzer, J. G. Wildenbeest, D. M. Weinberger, L. Bont, Surveillance of Pediatric REspiratory Admissions in Dutch hospitals (SPREAD) Study Group, Year-Round Respiratory Syncytial Virus Transmission in The Netherlands Following the COVID-19 Pandemic: A Prospective Nationwide Observational and Modeling Study. *J. Infect. Dis.* **228**, 1394–1399 (2023).

39. J. R. Hamilton, D. Sachs, J. K. Lim, R. A. Langlois, P. Palese, N. S. Heaton, Club cells surviving influenza A virus infection induce temporary nonspecific antiviral immunity. *Proc. Natl. Acad. Sci. U. S. A.* **113**, 3861–3866 (2016).

40. C. A. Johnson-Delaney, S. E. Orosz, *Vet. Clin. North Am. Exot. Anim. Pract.*, in press.

41. Y. Cao, Y. Huang, K. Xu, Y. Liu, X. Li, Y. Xu, W. Zhong, P. Hao, Differential responses of innate immunity triggered by different subtypes of influenza a viruses in human and avian hosts. *BMC Med. Genomics*. **10**, 70 (2017).

42. J. van Summeren, A. Meijer, G. Aspelund, J. S. Casalegno, G. Erna, U. Hoang, B. Lina, VRS study group in Lyon, S. de Lusignan, A. C. Teirlinck, V. Thors, J. Paget, Low levels of respiratory syncytial virus activity in Europe during the 2020/21 season: what can we expect in the coming summer and autumn/winter? *Euro Surveill.* **26** (2021), doi:10.2807/1560-7917.ES.2021.26.29.2100639.

43. D. K. Yeoh, D. A. Foley, C. A. Minney-Smith, A. C. Martin, A. O. Mace, C. T. Sikazwe, H. Le, A. Levy, C. C. Blyth, H. C. Moore, Impact of Coronavirus Disease 2019 Public Health Measures on Detections of Influenza and Respiratory Syncytial Virus in Children During the 2020 Australian Winter. *Clin. Infect. Dis.* **72**, 2199–2202 (2021).

44. J. Mereckiene, S. Cotter, J. T. Weber, A. Nicoll, F. D'Ancona, P. L. Lopalco, K. Johansen, A. M. Wasley, P. Jorgensen, D. Lévy-Bruhl, C. Giambi, P. Stefanoff, L. Dematte, D. O'Flanagan, VENICE project gatekeepers group, Influenza A(H1N1)pdm09 vaccination policies and coverage in Europe. *Euro Surveill.* **17** (2012), doi:10.2807/ese.17.04.20064-en.

45. K. Hebbrecht, M. Stuivenga, T. Birkenhäger, M. Morrens, E. I. Fried, B. Sabbe, E. J. Giltay, Understanding personalized dynamics to inform precision medicine: a dynamic time warp analysis of 255 depressed inpatients. *BMC Med.* **18**, 400 (2020).

764 46. J. Mellor, C. E. Overton, M. Fyles, L. Chawner, J. Baxter, T. Baird, T. Ward,
765 Understanding the leading indicators of hospital admissions from COVID-19 across
766 successive waves in the UK. *Epidemiol. Infect.* **151**, e172 (2023).

767 47. L. Miralles-Pechuán, A. Kumar, A. L. Suárez-Cetrulo, Forecasting COVID-19 cases
768 using dynamic time warping and incremental machine learning methods. *Expert Syst.*
769 **40** (2023), doi:10.1111/exsy.13237.

770 48. J.-D. Morel, J.-M. Morel, L. Alvarez, Time warping between main epidemic time series in
771 epidemiological surveillance. *PLoS Comput. Biol.* **19**, e1011757 (2023).

772 49. Z. Luo, L. Zhang, N. Liu, Y. Wu, Time series clustering of COVID-19 pandemic-related
773 data. *Data Science and Management*. **6**, 79–87 (2023).

774 50. R. M. Anderson, H. Heesterbeek, D. Klinkenberg, T. D. Hollingsworth, How will country-
775 based mitigation measures influence the course of the COVID-19 epidemic? *Lancet*.
776 **395**, 931–934 (2020).

777 51. S. Sakleshpur, A. L. Steed, Influenza: Toward understanding the immune response in
778 the young. *Front Pediatr*. **10**, 953150 (2022).

779 52. R. M. Hamilton, R. E. Foster, T. J. Gibb, C. J. Johannsen, J. B. Santini, Pre-visible
780 Detection of Grub Feeding in Turfgrass using Remote Sensing. *Photogrammetric*
781 *Engineering & Remote Sensing*. **75**, 179–192 (2009).

782 53. P. Senin, Dynamic time warping algorithm review (2008) (available at
783 https://www.semanticscholar.org/paper/Dynamic-Time-Warping-Algorithm-Review-
784 Senin/8096fe77e22ee54d829861642ac71064d866b913).

785 54. T. Giorgino, Computing and Visualizing Dynamic Time Warping Alignments in R: The
786 dtw Package. *J. Stat. Softw.* **31**, 1–24 (2009).

787 55. G. De Serres, I. Rouleau, M. E. Hamelin, C. Quach, D. Skowronski, L. Flamand, N.
788 Boulianne, Y. Li, J. Carbonneau, A. Bourgault, M. Couillard, H. Charest, G. Boivin,
789 Contagious period for pandemic (H1N1) 2009. *Emerg. Infect. Dis.* **16**, 783–788 (2010).

790 56. L. F. White, J. Wallinga, L. Finelli, C. Reed, S. Riley, M. Lipsitch, M. Pagano, Estimation
791 of the reproductive number and the serial interval in early phase of the 2009 influenza
792 A/H1N1 pandemic in the USA. *Influenza Other Respi. Viruses*. **3**, 267–276 (2009).

793

794

795 **Acknowledgments:** This work was supported by a grant from the National Institutes of

796 Health (R01AI137093). The content is solely the responsibility of the authors and does not

797 necessarily represent the official views of the National Institutes of Health.

798

799 **Author contribution:**

800 Conceptualization; KL, DMW, VEP

Data curation; KL

Formal analysis; KL, DMW, VEP

Funding acquisition; DMW, VEP

Methodology; KL, DMW, VEP

Software; KL

Supervision; DMW, VEP

Visualization; KL

Writing - original draft; KL

Writing - review & editing; KL, DT, DMW, VEP

All authors read and approved the final manuscript.

Competing interests: DMW has been principal investigator on grants from Pfizer and Merck to Yale University for work unrelated to this manuscript and has received consulting and/or speaking fees from Pfizer, Merck, and GSK/Affinivax. The other authors declare no competing interests.

Data and availability： All visualization was performed in R (version 4.0.2), and code to produce all figures and data used in this analysis are available in the GitHub repository https://github.com/keli5734/viral-interference.

Figures

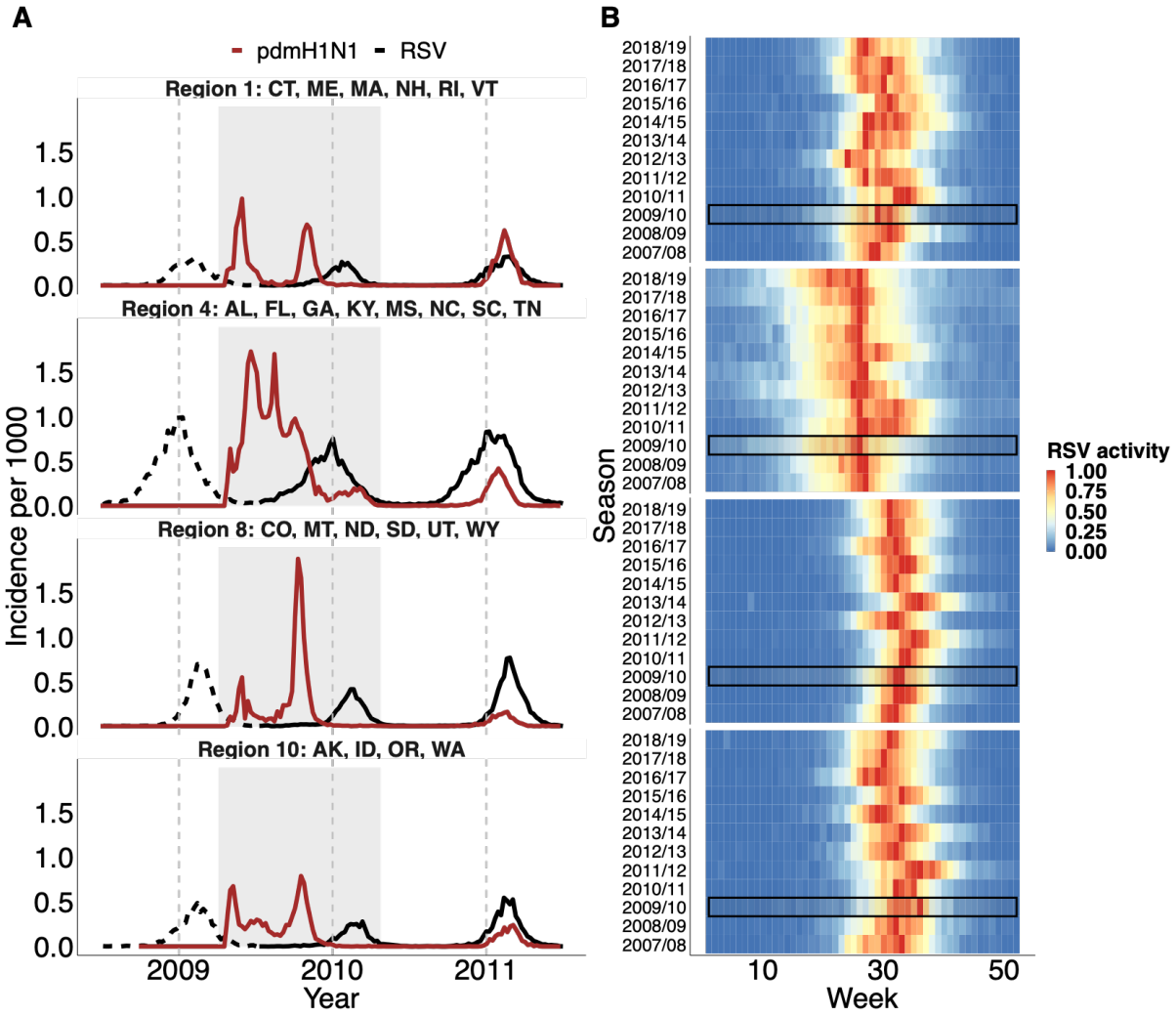

Fig. 1. Laboratory-confirmed positive tests for pdmH1N1 virus and RSV following the pandemic.

(A) Positive laboratory tests for pdmH1N1 virus (red) and RSV (black) before (dashed line), during (shaded area) and following the 2009 influenza pandemic in Region 1 (CT: Connecticut, ME: Maine, MA: Massachusetts, NH: New Hampshire, RI: Rhode Island, VT: Vermont), Region 4 (AL: Alabama, FL: Florida, GA: Georgia, KY: Kentucky, MS: Mississippi, NC: North Carolina, SC: South Carolina, TN: Tennessee) Region 8 (CO: Colorado, MT: Montana, ND: North Dakota, SD: South Dakota, UT: Utah, WY: Wyoming) and Region 10 (AK: Alaska, ID: Idaho, OR: Oregon, WA: Washington) of the US. Dashed gray lines indicate the 1st of January each year. **(B)** Heatmap of RSV activity by epidemic season for the four selected regions. Epidemic seasons are defined as starting in July and ending in June of the following year. RSV activity was calculated as the fraction of positive tests among the total number of tests for each season. The resulting fraction was then normalized to a range between 0 and 1,

with red indicating high activity and blue indicating low activity. RSV activity during the pandemic 2009/10 season is highlighted in the black box.

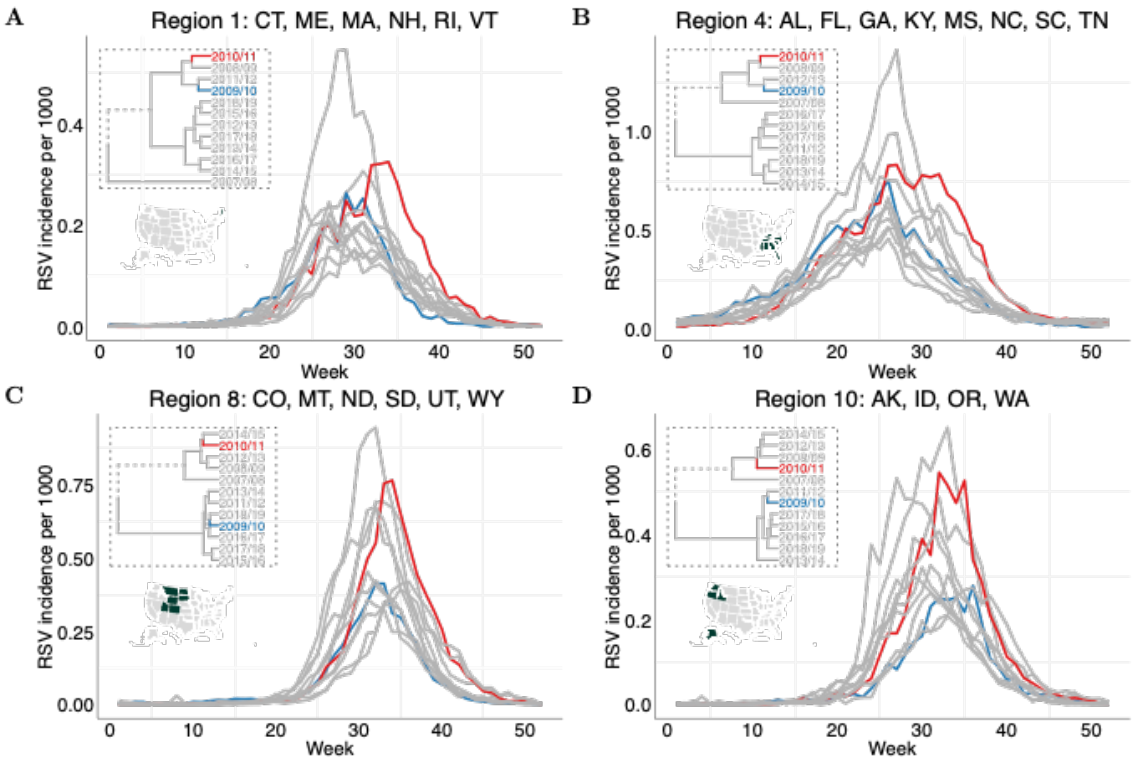

Fig. 2. Hierarchical clusters and RSV time-series in the four selected regions.
An agglomerative clustering algorithm with a Ward variance method was used to group the 12 RSV epidemic seasons in each region based on the alignment paths (**Fig. S2**). The dendrograms (in the dashed box) give the clustering results based on the optimal alignments between time-series computed by DTW. **(A)-(D)** show the dendrogram and corresponding RSV time-series in Regions 1, 4, 8 and 10, respectively. RSV time-series following the pandemic seasons are highlighted in blue (2009/10) and red (2010/11). The clustering results for other regions are given in **Fig. S3**.

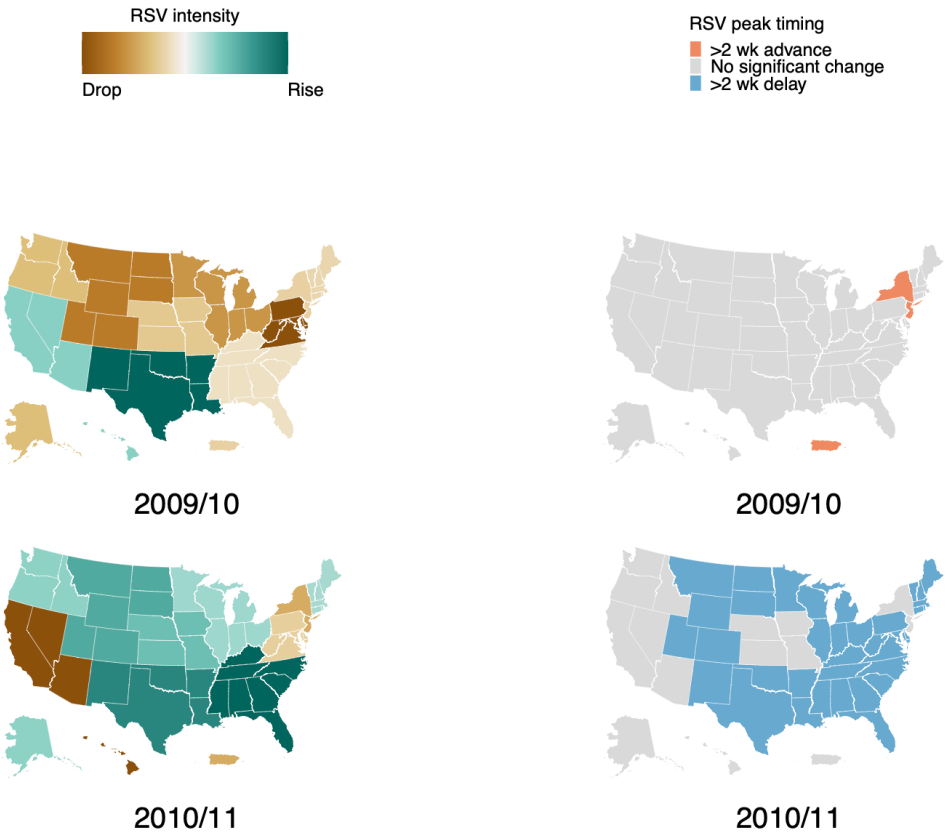

Fig. 3. The changes in RSV intensity and the center of gravity of RSV activity following the pandemic.

RSV intensity and the center of gravity of RSV activity were calculated for each epidemic season in each region of the US individually. For each region, the changes in the intensity of RSV activity in either the 2009/10 or 2010/11 season (i.e., query) were compared to the median values of all other seasons (i.e., reference), such that intensity changes = (query − reference) / reference × 100%. The changes in the center of gravity were given by the difference between the RSV-weighted weekly average for the query and the reference.

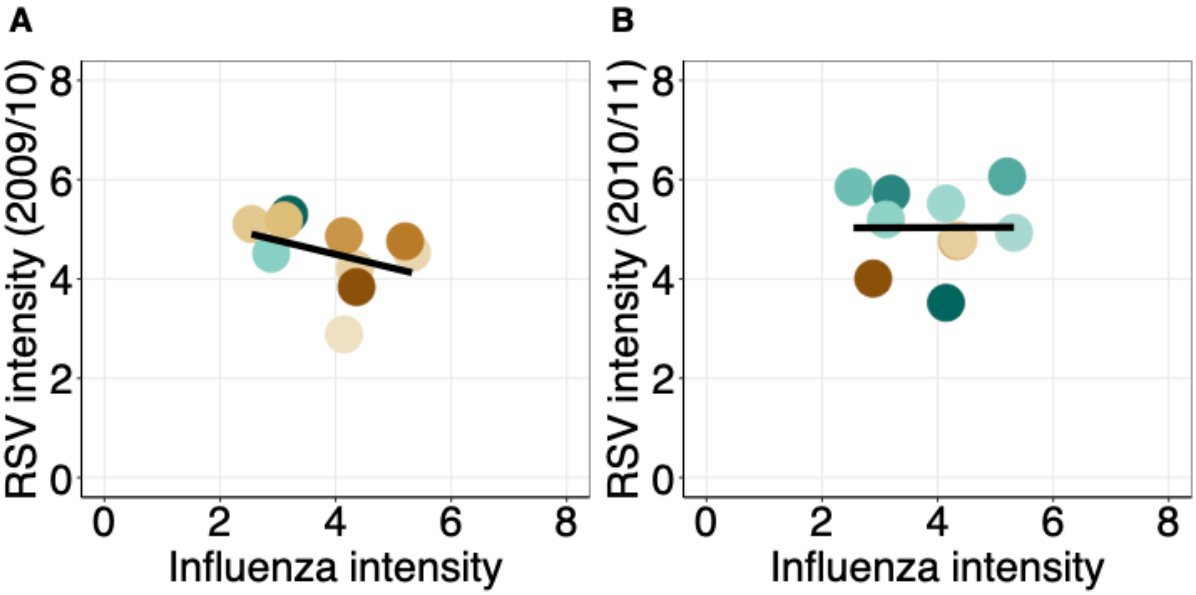

Fig. 4. Correlations between RSV intensity and pdmH1N1 virus intensity.
(A) The correlation between the intensity of RSV in the 2009/10 season and the intensity of pdmH1N1 virus during the pandemic period ($\rho = -0.38$), and **(B)** the correlation between the intensity of RSV in the 2010/11 season and the intensity of pdmH1N1 virus during the pandemic period ($\rho = 0$). The colors indicate the drop (brown) or rise (green) of RSV intensity in certain regions, corresponding to the US map in **Fig. 3**.

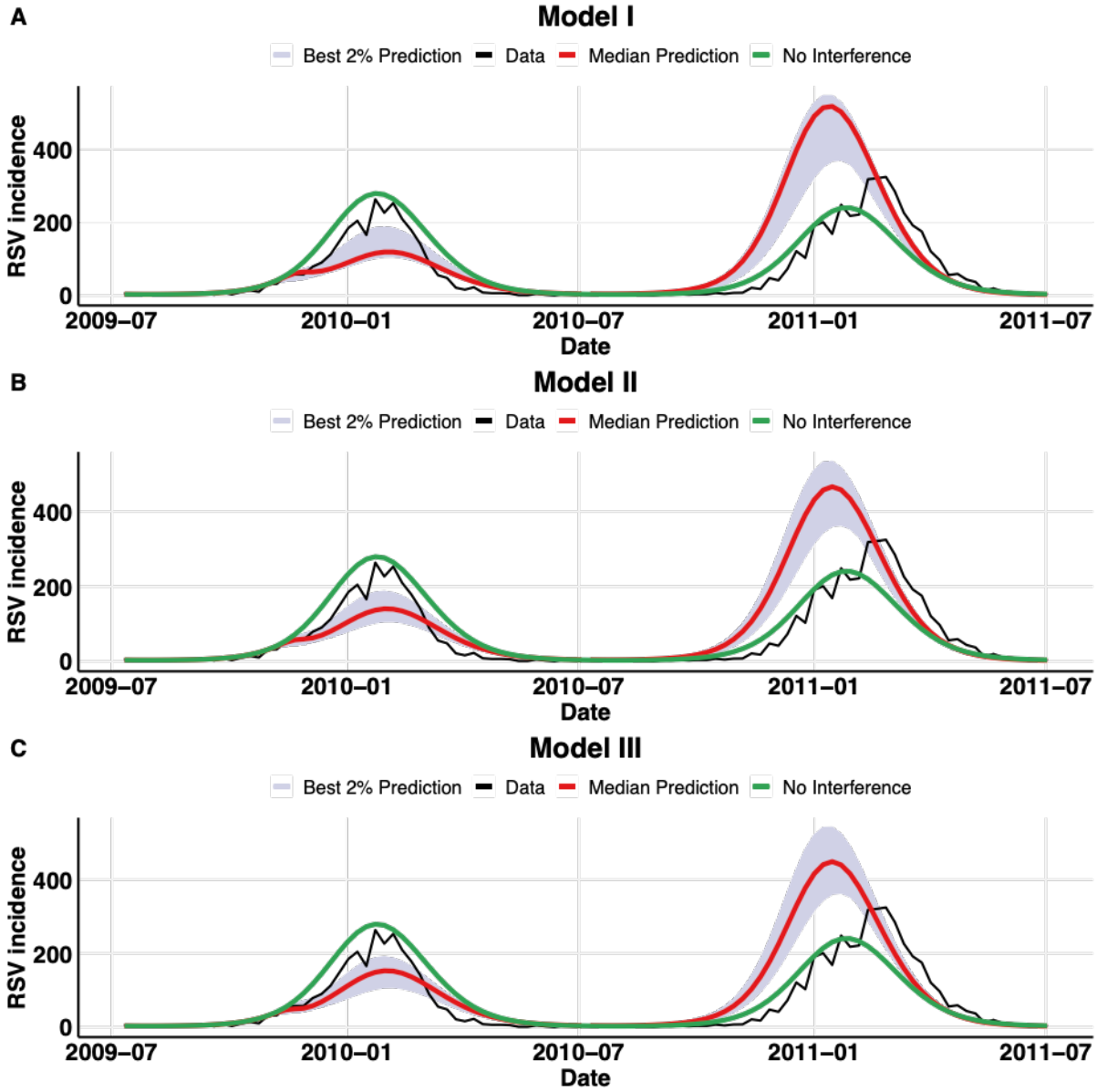

Fig. 5. Results of model fits for laboratory-confirmed RSV-positive tests in the 2009/10 and 2010/11 seasons in Region 1.

The observed number of RSV-positive tests in Region 1 is shown by the black line, while the top 2% of best-fitting models (based on 100,000 models generated from Latin Hypercube Sampling) is shown by the gray shaded region for **(A)** Model I—pdmH1N1 infection reduces susceptibility of RSV infection, **(B)** Model II—pdmH1N1 infection reduces RSV infectious period, and **(C)** Model III—pdmH1N1 infection reduces RSV infectivity. The median prediction, given by the median estimates of the viral interference parameter and associated other parameters, is indicated by the red curve. The green curve shows the scenario of no viral interference. Note that the models were only fitted to the RSV incidence data in the 2009/10 season, and the data from the 2010/11 season were used for model validation.

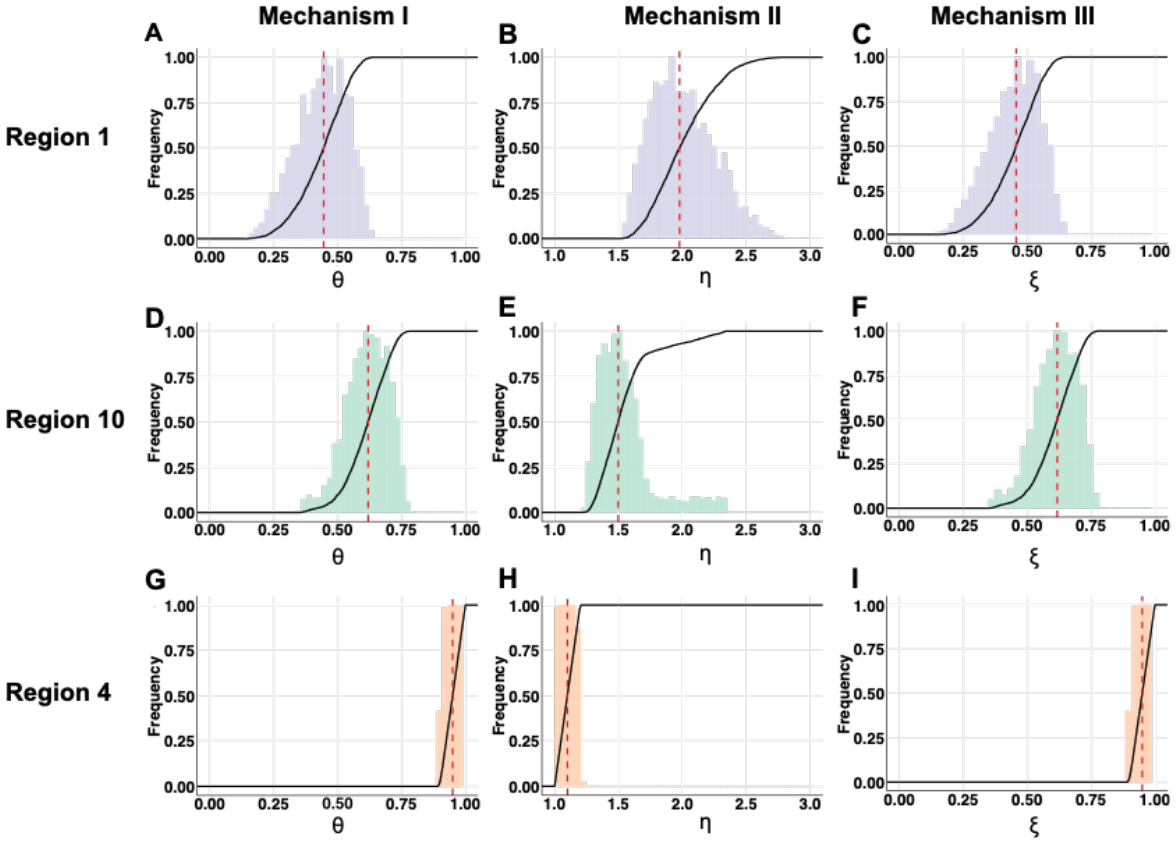

Fig. 6. Identified parameter space for viral interference parameters.
Histograms show the frequency of the values of viral interference parameters for the top 2% best-fitting models (2000 samples). The cumulative density functions (CDFs) are given by the solid lines, and the dashed red lines indicate the median estimates. **(A, D, G)** show the identified parameter distribution for the viral interference mechanism that reduces the host's susceptibility to RSV infection, θ (Model I), in Region 1, 10 and 4, respectively. **(B, E, H)** show the identified parameter distribution for the viral interference mechanism that shortens RSV infectious period, η (Model II), in Region 1, 10 and 4, respectively. **(C, F, I)** show the identified parameter distribution for the viral interference mechanism that reduces RSV infectivity, ξ (Model III), in Region 1, 10 and 4, respectively.